Covalent interactions in alloys of transition metals with simple metals or metalloids

1991 J. Phys.: Condens. Matter 3 9579

(http://iopscience.iop.org/0953-8984/3/48/001)

J. Phys.: Condens. Matter 3 (1991) 9579–9596. Printed in the UK

REVIEW ARTICLE

Covalent interactions in alloys of transition metals with simple metals or metalloids

J F van Acker, E W Lindeyer and J C Fuggle

Research Institute of Materials, University of Nijmegen, Toernooiveld, 6525 ED Nijmegen, The Netherlands

Received 10 December 1990

Abstract. The covalent interaction between localized transition metal d states and extended metalloid sp states, which plays an important role in the formation of alloys of transition metals with simple metals or metalloids, is considered from the point of view of the Anderson impurity model. We demonstrate how by means of concepts derived from this impurity model a basic understanding of the electronic structure of transition metal–metalloid alloys can be obtained. In addition, the experimental investigation of the electronic structure of such compounds by means of high-energy spectroscopies is discussed. In particular, we consider the interpretation of experimental results from photoelectron spectroscopy and x-ray absorption spectroscopy.

1. Introduction

This study describes various aspects of covalency, i.e. the interaction between nearly degenerate states, in alloys of transition metals with sp metals or metalloids. Without pretending to be an exhaustive review article it provides an overview of the applicability of concepts derived from impurity models and of the role to be played by some high-energy spectroscopies.

Bonding between transition metals and simple metals or metalloids (in particular Al, B and Si) is largely determined by the interaction between sp-like states and transition metal d states. Insight in the mechanism of the sp–d hybridization is therefore important for an understanding of the electronic structure and, for example, the structural and magnetic properties of such compounds [1–3]. There is a remarkably strong similarity in the shape of the density of states (DOS) of these materials, irrespective of the diversity in crystal structures. The overall distribution of states consists of a relatively narrow transition metal d band within a broad band of states of mainly s and p, but also some d symmetry. The extended band is moreover characterized by a typical hybridization gap at the position of the d band, which splits the sp states into a bonding and an antibonding part.

Evidence for this general scheme has been obtained from comparative theoretical and experimental investigation involving self-consistent band structure calculations and high-energy spectroscopy [4–15]. The experimental investigation of the electronic structure of these specific materials has focused mainly on the occupied states by means of x-ray photoelectron spectroscopy (XPS) [5–7, 13–15] low-energy photoemission spectroscopy [8] and x-ray emission spectroscopy (XES) [4, 5, 11, 14]. More recent

0953-8984/91/489579+18$03.50

studies emphasize the status of the unoccupied part of the band, using Bremsstrahlung isochromat spectroscopy (BIS) [10, 13, 14] and x-ray absorption spectroscopy (XAS) [9, 10, 12].

The s–d hybridization appears as a basic parameter in the Anderson impurity model, which deals with the case of a transition metal impurity d state interacting with a conduction band [16]. The first formulation and subsequent development of this model have contributed enormously to a general understanding of the behaviour of 3d transition metal impurities, in particular in noble metal hosts (see, e.g., [17–20] and references therein). Using a formalism based on the Anderson impurity Hamiltonian, Terakura *et al* [1, 21] established a formal correspondence between the shape of the hybridization gap in the sp band and the Fano anti-resonance in optical absorption spectra [22]. The existence of a band gap is furthermore considered to explain the concentration dependence of the magnetization in transition metal–metalloid alloys, which to a high degree is structure insensitive [3].

Our first aim in this study is to show how an impurity model like the Anderson model [16] can be used to provide a basic understanding of the electronic structure of these specific materials. We will emphasize the covalent interaction between the impurity state and surrounding host states and, in addition, consider the magnetic behaviour of an impurity interacting with the non-magnetic host. Concepts thus developed will be transferred to the case of the concentrated alloy and discussed in particular for AlPd.

Our second purpose is to deal with the interpretation of experimental data from high-energy spectroscopy, generally considered as a probe of the local electronic structure of the solid state. We therefore first discuss the photoionization process in more detail and stress the importance of cross section effects. Valence band photoemission spectra of the dilute alloy AuNi, of the compound AlPd and of the Ni–B metal–metalloid alloys are presented in order to support the discussion. Finally, we deal with the empty states and their spectroscopy XAS, exemplified by means of experimental data from Ni and Ni borides.

2. The interaction between d and sp states

Before discussing the concentrated alloy, we will, in this section, first consider the impurity limit and deal with the Anderson impurity Hamiltonian.

2.1. The Anderson impurity model

The Hamiltonian of the non-degenerate version of the Anderson impurity model is given by [16]

$$H = \sum_{\sigma,k} \varepsilon_k a^\dagger_{k\sigma} a_{k\sigma} + \varepsilon_d \sum_\sigma d^\dagger_\sigma d_\sigma + \sum_{\sigma,k} (V_{dk} d^\dagger_\sigma a_{k\sigma} + V_{kd} a^\dagger_{k\sigma} d_\sigma) + U n_{d\uparrow} n_{d\downarrow} \qquad (1)$$

where d_σ and $a_{k\sigma}$ are the annihilation operators for the d state and sp states respectively, ε_k describes the dispersion of the conduction band, ε_d is the energy level of the impurity state, and V_{dk} is the hybridization matrix element coupling the impurity level and the extended states. The electron–electron interaction is included by means

of the Coulomb correlation term U and will be discussed further in section 2.3. In the non-magnetic case ($U = 0$) the on-site impurity Green's function can be expressed as

$$G_{dd}(\varepsilon) = [z - \varepsilon_d - \Sigma(\varepsilon)]^{-1} \tag{2}$$

where

$$\Sigma(\varepsilon) = \sum_k \frac{V_{dk}V_{kd}}{z - \varepsilon_k} \tag{3}$$

and $z = \varepsilon + i0$. When the energy dependence of the interaction term is neglected, or $\Sigma(\varepsilon) = \Delta + i\Gamma$, the shape of the local density of states (LDOS) at the impurity site is Lorentzian:

$$n(\varepsilon) = -\frac{1}{\pi}\mathrm{Im}\{G_{dd}(\varepsilon)\} = \frac{1}{\pi}\frac{\Gamma}{(\varepsilon - \varepsilon_d - \Delta)^2 + \Gamma^2}. \tag{4}$$

The perturbation of the d state because of the covalent interaction with the sp band can thus be understood as a shift Δ of the impurity resonance and a broadening with halfwidth parameter Γ. The broadening of the atomic d state to a virtual bound state (VBS) can be understood in accordance with the golden rule as a transition rate coupling the localized d level and the free-electron-like states:

$$\Gamma = \pi V_{\mathrm{eff}}^2 n_H(\varepsilon_d) \tag{5}$$

where $n_H(\varepsilon_d)$ is the host DOS at the energy position of the impurity.

Assuming the mean square matrix element $|V_{dk}|^2$ to be k independent, we replace it by an effective constant parameter V^2. This yields [17]

$$G_{dd}(\varepsilon) = [z - \varepsilon_d - V^2 g(\varepsilon)]^{-1}. \tag{6}$$

Here $g(\varepsilon)$ is the normalized unperturbed host Green's function. In figure 1 the LDOS at the impurity site in case of interaction with a free-electron-like DOS is shown for two positions of the atomic level of the impurity state. The interaction parameter V is assumed to be equal in both cases. It is observed that the VBS is broader if the host DOS at the position of the impurity is larger, and that the peak position of the VBS is slightly shifted with respect to the atomic level (indicated by arrows in figure 1), as can be understood from equation (4). States having an impurity character are distributed over the total energy range of the host DOS because of the covalent interaction. In addition, the LDOS is not exactly Lorentzian, but slightly distorted because of the parabolic shape of the host band.

2.2. Covalent interaction and screening

Apart from the LDOS at the impurity site, the Anderson impurity model allows the calculation of the induced change in the DOS of the host band as

$$\delta n(\varepsilon) = \frac{1}{\pi}\mathrm{Im}\left\{V^2 G_{dd}(\varepsilon)\frac{\partial g(\varepsilon)}{\partial \varepsilon}\right\}. \tag{7}$$

This redistribution of the sp states is a consequence of the covalent interaction with the localized impurity state. Its asymmetric, anti-resonance-like shape, which again is

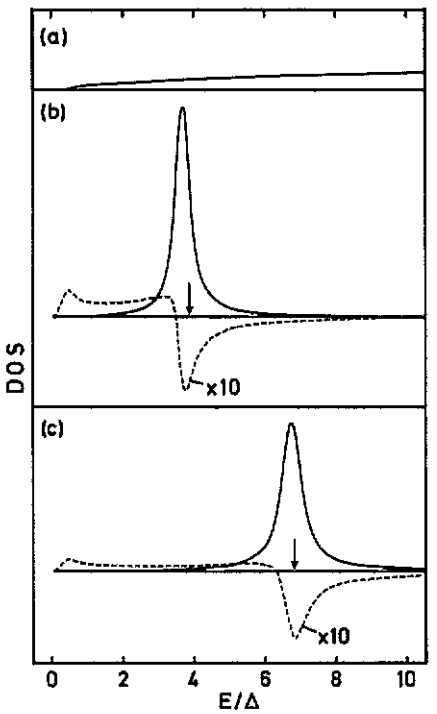

Figure 1. LDOS (full curve), calculated by means of the Anderson impurity model, for an impurity state interacting with a parabolic free electron-like band. Two positions (b and c) of the impurity level, indicated by arrows, have been chosen, while the s–d hybridization parameter is in both cases equal ($V = \Delta$). The broken curves show the induced change in the host DOS.

related to the parabolic shape of the free-electron-like host DOS, is shown in figure 1. It demonstrates that the hybridization gap in the sp band, which is a clear feature of the DOS of concentrated transition metal–metalloid alloys, does already develop for a single impurity in the lattice. Note that an infinitely broad band with a constant DOS is not affected by the impurity potential, since in that case $\partial g(\varepsilon)/\partial\varepsilon = 0$ (compensation theorem) [16].

If the change in the total DOS of the imperfect lattice, i.e. the sum of the impurity LDOS and the induced change in the DOS of the extended band, is integrated up to the Fermi level, one obtains the screening charge ΔZ. This is the total charge redistributed within the lattice in order to screen the localized perturbation. It obeys the Friedel sum rule [23]

$$\Delta Z = \frac{2}{\pi}\sum_{l}(2l+1)\delta_l(\varepsilon_F) \tag{8}$$

stating that the effective difference in nuclear charge at the impurity site is the sum of the screening contributions of the individual orbital channels. Each contribution is, apart from the orbital degeneracy, determined by the scattering phase shift at the Fermi level $\delta_l(\varepsilon_F)$. For a localized spherically symmetric perturbing potential embedded in a free-electron gas the asymptotic form of the radial part of the scattered wave is given by [24]

$$R_l(r) \propto \{\sin[kr - \tfrac{1}{2}l\pi + \delta_l(k)]\}/r. \tag{9}$$

A redistribution of charge density is associated with the perturbed wavefunction, and for large r it has the form:

$$\Delta\varrho_l(r) \propto \{\cos[2k_F r + \delta_l(k_F)]\}/r^3. \tag{10}$$

The charge density which screens the localized perturbing potential therefore shows long-range spatial oscillations, known as the Friedel oscillations.

2.3. The magnetic state

Next, we consider the case where $U \neq 0$. In the Hartree–Fock (HF) approximation we replace $Un_\uparrow n_\downarrow$ by $U\langle n_\uparrow\rangle n_\downarrow + Un_\uparrow\langle n_\downarrow\rangle$, and in this way obtain a single-particle Hamiltonian for each spin state [16]. As in equation (2) the spin-dependent LDOS is now given by

$$G_{dd\sigma}(\varepsilon) = [z - \varepsilon_d - U\langle n_{-\sigma}\rangle - V^2 g(\varepsilon)]^{-1}. \tag{11}$$

This defines the exchange splitting (the difference in effective level of both spin bands) as $\Delta_{ex} = Um$, where $m = \langle n_\uparrow\rangle - \langle n_\downarrow\rangle$ is the on-site magnetic moment. The HF self-consistency condition for the existence of a magnetic state is expressed as (see, e.g., [17])

$$m = -\frac{1}{\pi}\int^{\varepsilon_F} \mathrm{Im}\{G_{dd\uparrow}(\varepsilon) - G_{dd\downarrow}(\varepsilon)\}\,\mathrm{d}\varepsilon \tag{12}$$

which only has a non-trivial solution for

$$\frac{U}{\pi}\int^{\varepsilon_F} \mathrm{Im}\{G^2_{ddn}(\varepsilon)\}\,\mathrm{d}\varepsilon > 1$$

where $G_{ddn}(\varepsilon)$ is the local Green's function in the non-magnetic (paramagnetic) state. If the shape of the impurity LDOS is Lorentzian, as expressed in equation (4), the condition for a magnetic state becomes

$$Un_n(\varepsilon_F) > 1 \tag{14}$$

where $n_n(\varepsilon_F)$ is the LDOS at the Fermi level in the non-magnetic state. For concentrated alloys a similar condition, known as the Stoner criterion, stresses the importance of the DOS at the Fermi level for magnetic properties. Note, however, that in the impurity case the appearance of a magnetic state has no bearing on the existence of long-range order.

Although the Anderson model already in its non-degenerate form provides a clear insight into the magnetic behaviour of 3d impurities in noble metals [20], the HF approximation explicitly assumes a static mean field (or effective potential) for each spin state. It therefore neglects the local spin fluctuations, which tend to diffuse the sharp theoretical boundary appearing in equation (13) between the magnetic and non-magnetic case, and which are caused by such phenomena as inelastic and spin–flip scattering of conduction electrons [18]. In addition, the HF approximation does not

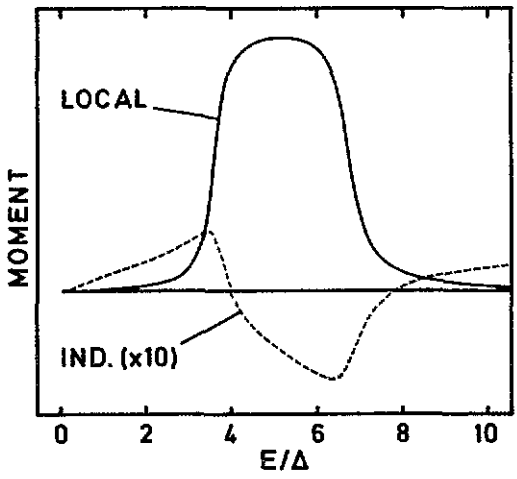

Figure 2. Local and induced moment as a function of the position of the Fermi level for the magnetic impurity system modelled in figure 1 (b and c). Explanation in text.

necessarily give a correct description of the situation at zero temperature, since the s–d exchange interaction may quench the local magnetic moment through the formation of a singlet bound state with the conduction electrons (Kondo effect) [19].

Within the HF approximation the screening mechanism is treated per spin state as in the non-magnetic case (section 2.2). Majority and minority spin states may therefore be associated with different screening charges and the covalent admixture between impurity and host states is thus, in general, the cause of an induced magnetic moment in the host. Here we refer again to figure 1, which we now interpret as the hypothetical case of a magnetic impurity state interacting with a free electron DOS. The hybridization parameter V has thus been chosen equal for both majority (figure 1(*b*)) and minority (figure 1(*c*)) spin states. From the local and induced redistribution of states the local and induced magnetic moment for this particular system can be obtained as a function of the position of the Fermi level (figure 2). The important aspect here is the sign of the induced magnetic polarization, which may be positive (ferromagnetic) or negative (antiferromagnetic), depending on the position of the Fermi level in the band. As indicated in figure 2 the net effect of a magnetic moment, induced by covalent interaction, appears to be generally small. However, it becomes significant if the magnetic susceptibility of the host material is exchange enhanced. In that case the un-enhanced induced magnetic moment may be multiplied by the enhancement factor [17]. The so-called giant magnetic moments caused by 3d impurities in Pd are the most remarkable examples of this magnetic enhancement of covalent interaction [25].

Friedel oscillations in the spatial distribution of the screening charge around the impurity appear in the magnetic case as spin density oscillations, and can be identified with the so-called Ruderman–Kittel–Kasuya–Yosida (RKKY) oscillations [26]. The spatial extent of these oscillations is considerable as follows from equation (10). The magnetic polarization brought about by a covalent admixture between impurity and host states is therefore more effective than the direct exchange interaction.

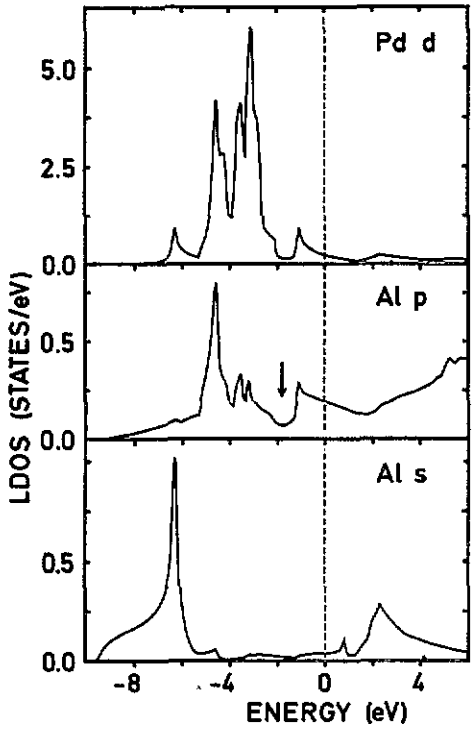

Figure 3. Self-consistently calculated Pd d and Al s and p partial DOS for AlPd. The arrow indicates the hybridization gap in the Al p partial DOS.

2.4. Interacting bands

Next, we will examine in how far the concepts developed in the preceding sections can be applied to the case of concentrated alloys. Figure 3 shows the Al s, p and Pd d partial DOS of AlPd, calculated self-consistently in the cubic CsCl crystal structure by means of the augmented spherical wave (ASW) formalism [7]. This alloy provides a particularly suitable example of the type of compound we have in mind. Most of the rapid fluctuations in the DOS are caused by van Hove singularities, but, in addition, trends with a slower energy dependence are observed. The Pd 4d band is characterized by a broad peak which tails off on both sides. The main structure is about 2.5 eV wide, and thus is considerably narrower than for the pure metal [27]. The cause of this band narrowing is partly the reduced Pd–Pd coordination number (from twelve in Pd metal to six in the alloy [7]), partly the increase of the Pd–Pd interatomic distance (from 2.75 Å in Pd metal to 2.99 Å in PdAl) [28]. The sp–d hybridization with the Al states, however, sets a limit to the process of band-narrowing. We thus observe a strong similarity with interacting states at the level of the Anderson impurity model, which explains the Lorentzian appearance of the Pd d band in AlPd and the spreading of d character into the unoccupied levels.

The shape of the Al sp band in AlPd is also quite different from its free-electron-like shape in Al metal [27]. The interaction with Pd 4d states results in an accumulation of bonding states of Al s character at the bottom of band, and a spreading of the, largely empty, antibonding states over a broader energy range. For the Al p band the redistribution of states in a bonding and antibonding portion and the position of a hybridization gap (at about 2 eV below the Fermi level) in between is somewhat

better defined. This division in bonding and antibonding states agrees with the bond order, which changes sign at the position of the anti-resonance [1]. A fully developed hybridization gap is thus observed, the first traces of which are demonstrated by the Anderson impurity model.

The hybridization gap in the s and p states, as well as the strong narrowing of the transition metal d band upon alloying can in a simple way be demonstrated by comparison with results of a band structure calculation that replaces the transition metal or metalloid sites by empty spheres. Although the position of the anti-resonance (or the minimum in the hybridization gap) and the position of the d resonance do practically coincide within the formalism of the Anderson impurity model, this is not necessarily the case for concentrated alloys [1, 21]. Within a tight-binding picture of the solid state this can be illustrated by means of a simple interacting band model, that collects the full interaction between d-like and s-like states in a single effective hybridization parameter V. The perturbed Green's function of the d band $G_d(\varepsilon)$ can then be given as

$$G_d(\varepsilon) = \frac{g_d(\varepsilon)}{1 - V^2 g_s(\varepsilon) g_d(\varepsilon)} \qquad (15)$$

where $g_d(\varepsilon)$ and $g_s(\varepsilon)$ are the normalized, unperturbed Green's functions, associated with the d and s band respectively. Note that the Anderson model is the impurity limit of this interacting band model. Figure 4 shows the result of this approach for the interaction between an extended free-electron-like band and a localized semi-elliptical band representing the d states. The perturbed s band clearly shows the hybridization gap and the accumulation of bonding states at the bottom of band. As a consequence of the covalent interaction, the d band has strongly broadened by spreading over the complete energy range of the extended band. Finally, a strong redistribution of weight within the d band has caused its main peak to move to a position different from that of the minimum in the hybridization gap. Interesting trends in the position and depth of the hybridization, or quasi-gap over the periodic system appear from the self-consistent band structure calculations of transition metal silicides, performed in recent years [8, 13].

Another effect, notable when comparing the Pd d partial DOS in the pure metal [27] with that of the alloy is the shift of the main structure of the d band to a lower energy with respect to the Fermi level and the strong decrease in the DOS at the Fermi level of the 4d states (in Pd 2.28 states/eV; in AlPd 0.22 states/eV). This effect, termed band filling, is not a matter of charge transfer, as one would expect of the alloying of Pd with electropositive Al, but is mainly the result of the covalent interaction between 4d and sp states (see, e.g., [11] and references therein). When the actual number of d electrons on the Pd site is considered the differences are small: 8.74 in elemental Pd compared with 8.86 in AlPd. Note that because of the decreased DOS at the Fermi level, band filling does not favour the existence of a magnetic state. This applies in particular to the Ni–metalloid alloy systems.

It is common practice to divide the d band of the alloy into a bonding and antibonding portion on both sides of the hybridization gap. The peaked region of the d band is often termed non-bonding, in which case one argues that it results from an interaction exclusively between those transition metal d states which by reason of symmetry are not allowed to mix with the sp states [2]. The distinct contribution of such purely non-bonding states to the d band is, however, not always clear [14], and

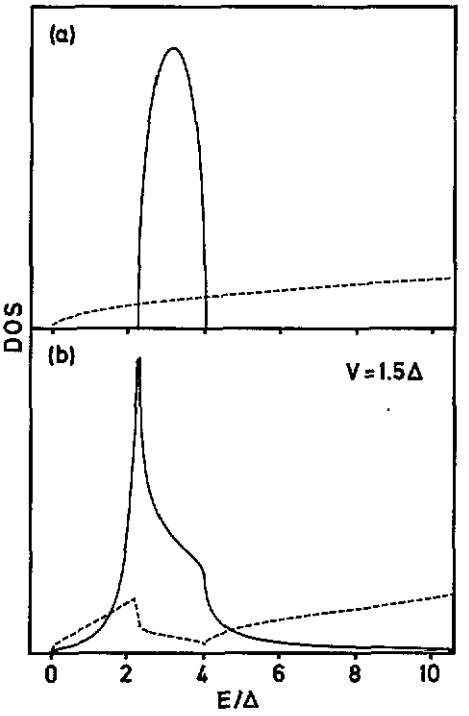

Figure 4. Simple model of an interacting parabolic free-electron-like band and a semi-elliptical d-like band.

that such a band of non-bonding states exists at all does not necessarily follow from the scheme that we have developed here.

3. High-energy spectroscopy

We will in this section first deal with general concepts concerning the photoemission process (for a more complete review see, for example, [29] and references therein) before discussing experimental results of high-energy spectroscopies in more detail.

3.1. Photoemission

The photoionization transition rate is given by Fermi's golden rule as

$$w_{\mathrm{fi}}(\omega) = \frac{2\pi}{\hbar}|\langle \mathrm{f}(N)|H'|\mathrm{i}(N)\rangle|^2 \delta(\varepsilon_{\mathrm{f}} - \varepsilon_{\mathrm{i}} - \hbar\omega) \tag{16}$$

where $|\mathrm{i}(N)\rangle$ and $|\mathrm{f}(N)\rangle$ are the N-particle initial and final states having energy ε_{i} and ε_{f} respectively. H' represents the operator coupling the electron momentum $\boldsymbol{p}$ and photon field $\boldsymbol{A}$ as

$$H' = \sum_j \frac{e}{2mc} \boldsymbol{A} \cdot \boldsymbol{p}_j. \tag{17}$$

In photoemission spectroscopy it is convenient to assume the outgoing photoelectron to be decoupled from the remaining system (sudden approximation). The photoemission intensity $I_{fi}(\omega)$ is then proportional to

$$I_{fi}(\omega) \propto |\langle f(N-1)|i(N-1)\rangle|^2 |\langle \phi_f|\boldsymbol{A}\cdot\boldsymbol{p}|\phi_i\rangle|^2 \delta(\varepsilon_f - \varepsilon_i - \hbar\omega). \tag{18}$$

Here $|i(N-1)\rangle$ and $|f(N-1)\rangle$ are the initial and final states associated with the $N-1$ spectator electrons and $|\phi_i\rangle$ and $|\phi_f\rangle$ are the one-electron wavefunctions of the photoelectron in the initial and final (continuum) states. The dependence of the photoemission transition rate on final state energy is therefore separated out in a one-electron matrix element, which is usually ignored in core level XPS because of its slow energy dependence.

In the atomic limit the one-electron matrix element can be expressed in terms of an atomic subshell photoionization cross section [30]

$$\sigma_{nl}(h\nu) = \frac{4\pi^2\alpha_0 a_0^2}{3}\frac{N_{nl}}{2l+1}h\nu[lR_{l-1}^2(\varepsilon_{kin}) + (l+1)R_{l+1}^2(\varepsilon_{kin})] \tag{19}$$

where ε_{kin} is the kinetic energy of the photoelectron and $R_{l\pm1}(\varepsilon_{kin})$ is the one-electron radial dipole matrix element, which in the dipole length approximation is expressed as

$$R_{l\pm1}(\varepsilon) = \int_0^\infty P_{nl}(r) r P_{\varepsilon,l\pm1}(r)\,\mathrm{d}r. \tag{20}$$

$P_{nl}(r)$ and $P_{\varepsilon,l\pm1}(r)$ represent the bound and continuum radial wavefunctions respectively. For other details we refer to the work by Yeh and Lindau [30]. Here we only wish to point out that the matrix element $R_{l\pm1}(\varepsilon)$ has $l-1$ as well as $l+1$ character in accordance with the dipole selection rules. The $l+1$ component will in general make the dominant contribution to the cross section [31]. However, if the initial state radial wavefunction has one or more nodes (e.g. in case of photoionization from 4d and 5d orbitals) the interesting situation may arise in which the overlap integral expressed in equation (20) cancels out. Accordingly, the photoionization cross section appears as a function of photon energy characterized by a distinct and rather broad minimum, known as the Cooper minimum [31].

In valence band photoelectron spectroscopy band structure effects are important. In terms of a one-electron formalism one can sum over initial and final states to obtain

$$I(\varepsilon) \propto \sum_{i,f}\int_{BZ} \mathrm{d}^3k |\langle\phi_f|\boldsymbol{A}\cdot\boldsymbol{p}|\phi_i\rangle|^2 \delta(\varepsilon_f(k) - \varepsilon_i(k) - \hbar\omega)\delta(\varepsilon - \varepsilon_i(k)) \tag{21}$$

where in the case of angle-integrated photoemission from a polycrystalline sample integration extends over the whole Brillouin zone. In addition to the condition of energy conservation equation (21) expresses the requirement of wavevector conservation in optical transitions. The latter requirement limits the availability of excitable initial states and is a cause of photon energy dependent structure in low-energy photoemission spectra of the valence band [32]. This condition is relaxed by increasing the photon energy ($h\nu > 100$ eV), which reduces final state structure and permits phonon-assisted transitions [33].

Using a muffin-tin description of the solid state, Winter *et al* [34] have expressed the photoemission transition rate at high photon energy (in particular for XPS) in the so-called single-site approximation as

$$I(\varepsilon) = \sum_l \sigma_l(\varepsilon) n_l(\varepsilon).$$

The photoemission intensity thus reproduces the site- and symmetry-projected partial DOS $n_l(\varepsilon)$, corrected by an energy-dependent orbital cross section $\sigma_l(\varepsilon)$. Formally the orbital cross section corresponds to its atomic counterpart as given by equation (18). The solid state contributions enter through its dependence on the muffin-tin potential. However, because of the strong contribution of the core region to the overlap integral the matrix element is predominantly atomic in character [35]. Solid state effects, therefore, only have a modulatory influence on the energy dependence of the photoionization cross section and may, for instance, change position and depth of the Cooper minimum [36].

This treatment suggests that the valence band photoemission probes, with appropriate correction for matrix elements, the DOS as calculated self-consistently using density functional theory and the local density approximation (LDA). Although the success of this approach can be considerable (see, e.g., [13]), it neglects the many-body effects that are associated with the excitation process and with the interacting hole. These effects can be incorporated by means of the so-called self-energy, $\Sigma_{kk}(\varepsilon)$, of the single hole state ([37, 38] and references therein). Apart from the cross section effects the spectral (quasi-particle) DOS $n'(\varepsilon)$ may then be written as

$$n'(\varepsilon) = -\frac{1}{\pi}\mathrm{Im}\{\sum_k G_{kk}(\varepsilon)\} \tag{23}$$

where $G_{kk}(\varepsilon) = [z - \varepsilon_k - \Sigma_{kk}(\varepsilon)]^{-1}$ is the diagonal matrix element of the single-particle Green's function. It is assumed here that the off-diagonal elements of the self-energy correction are negligibly small. The function $\Sigma_{kk}(\varepsilon)$ therefore acts as a generalized correction to the LDA eigenvalue ε_k. A small self-energy correction can, in formal equivalence with equation (4), be pictured as an energy shift with respect to the LDA eigenvalue, in addition to a lifetime broadening, associated with the excited final state. Self-energy corrections tend to be larger for states farther removed from the Fermi level and are partly responsible for the loss of structure in valence band photoemission spectra at higher binding energy. If pronounced, the energy dependence of $\Sigma_{kk}(\varepsilon)$ is the cause of satellite structure [39].

3.2. The valence band

The first experimental example we will show relates to the actual observation of impurity states by means of photoemission. Recent years have witnessed a considerable progress in the high-energy spectroscopic investigation of the local electronic structure of impurities in a variety of host materials. Such experimental data provide fairly direct information on the position and width of a VBS [40–44], on mixing between impurity and host states [42–44], and on magnetic interactions [42, 45].

Figure 5 shows low-energy photoemission spectra of the valence band of the dilute alloy AuNi (5 at.% Ni) at 65 and 170 eV [46]. These spectra provide a nice example of the power of the Cooper minimum effect in a photoemission investigation of dilute

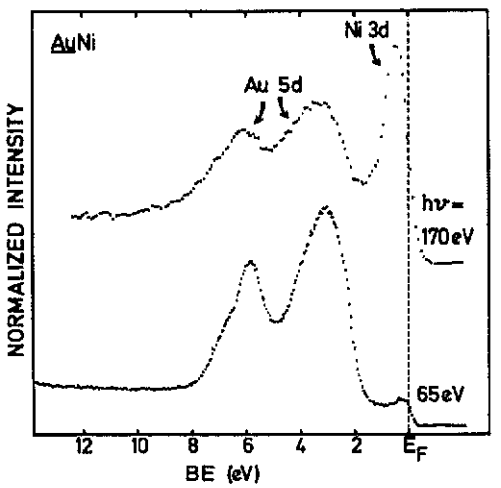

Figure 5. Low-energy valence band photoemission spectra of AuNi (5 at.% Ni), taken at 65 and 170 eV photon energy.

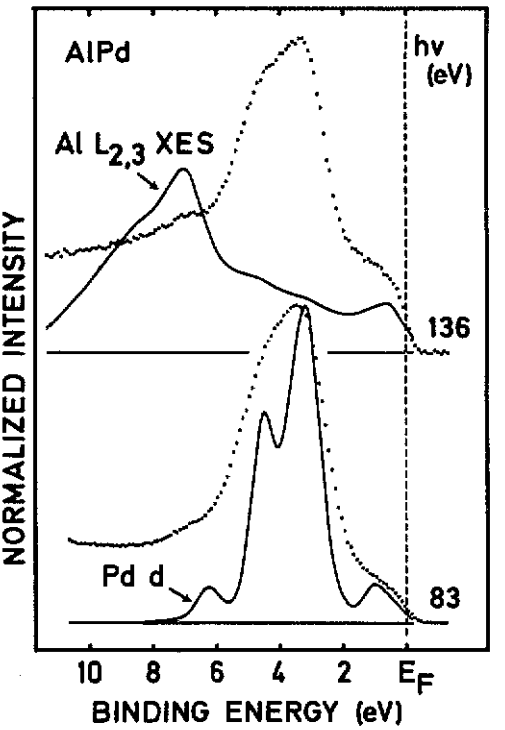

Figure 6. Low-energy photoemission data of the valence band of AlPd at 78 eV and at the Cooper minimum of the Pd 4d photoionization cross section (136 eV). Also inserted in the upper panel is the Al $L_{2,3}$ x-ray emission spectrum for AlPd [47]. The photoemission spectrum at 78 eV is compared with the broadened partial Pd d DOS.

alloys (see, for instance, [44–46]). In this case Au acts as an sp host to Ni because the Ni d level is situated in the Au sp band above the 5d band. We assume here that 5 at.% of random substitutional impurity atoms gives a reasonably accurate picture of the electronic properties in the dilute limit (although this may not always be the case). At 65 eV photon energy the spectrum is dominated by structures of the Au 5d band at approximately 5.5 and 8 eV. This picture changes dramatically around 170 eV photon energy, where the photoionization cross section of the Au 5d orbital has a Cooper minimum [30]. Photoemission originating from the Au 5d states is now strongly suppressed in favour of the Ni 3d impurity level, which at 0.4 eV binding energy dominates the spectrum. The width of the observed VBS is here predominantly due to instrumental broadening. On the basis of an ultraviolet photoelectron spectroscopy (UPS) study Bosch *et al* have concluded that the 3d resonance, which is spin degenerate (non-magnetic) and derives its width mainly from the covalent interaction with the Au sp band, should not be broader than 250 meV [41]. Mixing of Ni and Au d states has been experimentally demonstrated, but the effect is small because of the energy separation between the Au 5d band centroid and the Ni 3d level [44].

Low-energy photoemission spectra of the valence band of the concentrated alloy AlPd are presented in figure 7. Again, in order to emphasize the cross section effects

we show here data taken at 83 eV and at the Cooper minimum of the Pd 4d cross section (136 eV). At 83 eV the spectrum consists of a broad peak (at 3.5 eV binding energy) which tails off towards the Fermi level. It is dominated by the contribution of 4d states, which have a considerably higher cross section at this photon energy than the Al sp states [30]. The spectrum closely resembles the XPS valence band spectrum of AlPd, which also is known to reflect largely the contribution of 4d states [7]. Because of the better instrumental resolution in the low-energy photoemission experiment the d band is about 0.3 eV narrower. These data can be considered as a typical experimental observation of the electronic structure of a transition metal–metalloid compound, illustrating the concepts of band narrowing and band filling that occur when alloying Pd with electropositive Al. As shown in figure 7, a more detailed comparison with the self-consistently calculated Pd 4d partial DOS (dealt with in section 2.4), reveals that the experimental spectrum is broader than expected from instrumental effects alone, although the position of its centroid seems correctly reproduced in the calculation†. The small discrepancies are typically effects that may be interpreted as self-energy corrections to the self-consistently calculated ground state DOS. An understanding of these corrections is needed in order to obtain a better description of the photoemission process (cf section 3.1).

Because of the strongly suppressed contribution of the Pd 4d states, the photoemission data at 136 eV emphasize the extended shape of the Al sp band (with some Al d character mixed in), which is seen to host the more localized 4d band. Photoemission does not, however, provide a clearer view of the hybridization gap in s and p bands. Only a symmetry and site selective technique as XES allows for this. This is demonstrated by means of the Al $L_{2,3}$ x-ray emission spectrum of AlPd (data from [47]), which we have for comparison inserted in figure 6. Because of the dipole selection rules this spectrum reproduces mainly the distribution of the Al s states [7].

Finally, XPS valence band spectra of Ni and the borides Ni_3B, Ni_2B and NiB are presented in figure 7. The valence band of metallic Ni is characterized by its satellite at about 6 eV, which is associated with d^8-like final states. We do not intend a detailed comparison with band structure calculations here‡, but wish to demonstrate in the spectra a few trends that exist irrespective of the different crystal structures in which these borides form [49]. Because of the large difference in photoionization cross section between Ni 3d and B sp orbitals [30] the XPS data of the compounds primarily reflect the spectral distribution of the occupied Ni 3d states.

Although B is not electropositive with respect to Ni, we can nevertheless identify several trends that agree with the concept of d band filling. We propose that this arises because of covalent interaction with the B sp states as has been discussed, for example, in relation to XPS valence band spectra of intermetallics of Ni with electropositive Al [7]. With decreasing Ni concentration one observes: first, a shift of the main peak of the valence band (except in case of Ni_3B) to higher binding energy; second, a decrease of the DOS at the Fermi level; third a disappearance of the d^8-like satellite. In addition, the shape of the d band tends to become more symmetric. These observations also agree with the distribution of p-d bonding and antibonding states as concluded from B K x-ray emission data [11]. As in many other transition metal–metalloid systems, here also the process of Ni dilution is accompanied by the combined effect of a decreasing

† Matrix elements have, however, not been included in this comparison. Note, furthermore, that an erroneous energy scale in [7] has prompted these authors to a slightly different conclusion.

‡ A self-consistent calculation for Ni_3B, for example, can be found in [48].

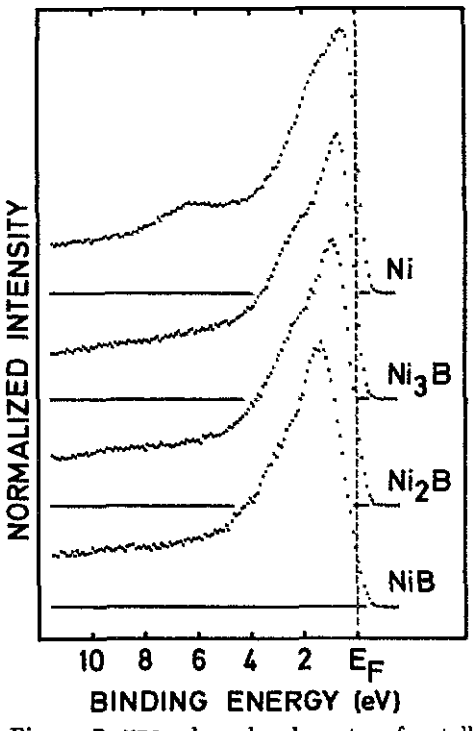

Figure 7. XPS valence band spectra of metallic Ni and the borides Ni_3B, Ni_2B and NiB.

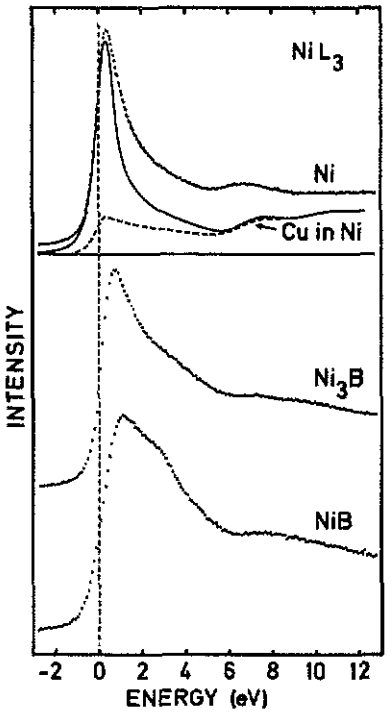

Figure 8. Ni L_3 XAS spectra of Ni metal and Ni borides (experimental data from F M F De-Groot), normalized to equal peak height. The edges are alligned by means of XPS binding energies of the $2p_{3/2}$ core levels. The spectrum of metallic Ni is compared with the calculated unoccupied d partial LDOS for pure Ni (full curve) and for a Cu impurity in Ni (broken curve).

Ni–Ni coordination number and an increasing Ni–Ni interatomic distance [49]. Because of the decreased DOS at the Fermi level the alloys have, in contrast to Ni metal, lost the ability to order magnetically ([3, 50] and references therein). Trends quite similar to the ones described earlier can also be identified in the XPS-BIS valence band spectra of transition metal silicides for example [13].

3.3. Unoccupied levels

In XAS photon impact causes the promotion of a core electron to an unoccupied state. This makes XAS a site selective spectroscopy. As in XPS the transition rate in XAS is given by Fermi's golden rule, expressed in equation (16). The dipole selection rules therefore in addition make XAS symmetry selective: only transitions to states of $l \pm 1$ symmetry are allowed.

In the case that band structure effects are considered important, reformulation in a one-electron formalism is appropriate. Summing over all (k-dependent) final states consistent with energy conservation results in an x-ray absorption yield $I(\omega)$

proportional to

$$I(\omega) \propto \int_{BZ} d^3k \, |\langle \phi_c | \boldsymbol{A} \cdot \boldsymbol{p} | \phi_k \rangle|^2 \delta(\hbar\omega - \varepsilon_c - \varepsilon_k) \tag{24}$$

where $|\phi_c\rangle$ and $|\phi_k\rangle$ are the one-electron atomic and final state wavefunctions with energy ε_c and ε_k respectively. Note that in this formalism many-body effects, like the Mahan–Nozières–de Dominicis edge singularity [51], are ignored. Using a muffin-tin description of the potential Müller *et al* [52] have shown that equation (24) can be approximated as

$$I(\varepsilon) \propto |M(\varepsilon)|^2 n(\varepsilon) \tag{25}$$

where $M(\varepsilon)$ is a single-particle matrix element, which expresses the energy dependence of the radial part of the final state wavefunction inside the muffin-tin sphere, and $n(\varepsilon)$ is the unoccupied DOS of appropriate symmetry.

Ni L_3 x-ray absorption edges of Ni, Ni_3B and NiB are presented in figure 8. Pure Ni is characterized by its narrow peak (white line) at the edge, followed by a plateau with a characteristic feature at 6.5 eV. The spectra of the borides also show enhanced intensity at the edge, but this intensity is more structured and distributed over a larger energy range (up to 5 eV). In accordance with the dipole selection rules we expect in these spectra to see contributions from the unoccupied Ni s as well as d states. On the other hand, we may assume that the d or $l+1$-like states dominate, because of the relative magnitude of the matrix elements, which in case of orbitals of d symmetry may be one or two orders of magnitude larger than the matrix elements associated with the s orbitals [9, 10, 12]. Our data therefore provide a picture of the unoccupied d levels at the Ni site. They are complementary to the XPS data in the preceding section and are compatible with the following scheme. The spectrum of pure Ni reflects the contribution of the unoccupied part of the Ni 3d band located just above the Fermi level. Comparison with the broadened unoccupied d partial DOS [27] in figure 8 seems to support this conclusion. Because of the covalent interaction with B sp states, alloying with B will result in a decrease of the DOS at the Fermi level and in spreading of Ni d symmetry across the unoccupied band.

In this analysis we have assumed that the XAS data reflect the distribution of unoccupied d states in the ground state. There remains the fact, which is at first surprising, that no effect of the core hole seems to be present in these x-ray absorption spectra. In $L_{2,3}$ edges of early 3d transition metals, for example, exchange and multipole effects have been found to dominate the spectra [53, 54]. Within a one-electron formalism the influence of the core hole on the spectral shape of the x-ray absorption edges can in general be understood in terms of an effective, attractive, potential [55, 56]. More recent evidence for the success of this approach has been obtained from Auger spectra of pure Si [57] and from the Si K (1s) x-ray absorption spectra of transition metal silicides [58].

The possible effect of a core hole in case of pure Ni has in figure 8 been indicated by comparing the L_3 XAS spectrum with the appropriately broadened unoccupied d DOS of a Cu impurity in Ni, calculated by means of the Korringa–Kohn–Rostoker Green's function formalism [59]. Our assumptions here include a completely relaxed final state (adiabatic approximation), and a $Z+1$ (or equivalent core) approximation to the core hole potential [60]. Although the matrix element has not been included, its (slow) energy dependence can certainly not be advanced as a possible cause of the

observed discrepancy with the experimental data. The L_3 edges of metallic Ni and the Ni borides therefore apparently agree with a general observation that for a nearly filled band the so-called final-state rule does not apply, and that comparison with the unperturbed, ground state DOS results in much better agreement. Experimental support for this conclusion has been obtained from the agreement between L_3 edges and BIS spectra (which are not affected by the presence of a core hole) for Ni metal [53, 61] and for Pd compounds [10]. In addition, first-principle calculations of the L_3 edges of Ni and Pd with neglect of the core hole effect give a satisfactory agreement with the experimental data [52, 62, 63]. Also from a purely theoretical point of view Grebennikov *et al* have suggested, that in the limit of zero unoccupied states the interaction with the core hole need not be taken into account [64].

4. Concluding remarks

We have demonstrated here how the Anderson impurity model can be used to obtain a basic understanding of the electronic structure of transition metal–metalloid alloys and, in particular, of the covalent interaction between sp and d states. Note that within this impurity scheme the LDOS at the transition metal site follows directly from the formalism of the model, while the incipient hybridization gap in the sp band is derived as an induced change in the *total* DOS of the conduction band. An apparently more direct indication that the LDOS at the metalloid site in a transition metal–metalloid alloy is characterized by a hybridization gap follows, again within an impurity formalism, from the reversed situation, that is by considering an sp impurity in a transition metal host [1, 65].

From a slightly different point of view this can be understood by considering, next to the Anderson model, the Clogston–Wolff impurity model [66], which was originally designed to explain the magnetic behaviour of a transition metal impurity in a transition metal host. This impurity model considers the covalent interaction between impurity and host d states assumed *a priori* nearly degenerate. In the original version of the Clogston–Wolff impurity model only the position of the impurity level is parametrized and the impurity-host d–d interaction is implicitly assumed to be equal to the unperturbed d-d interaction. A more recent, generalized version has removed this shortcoming [43, 67]. The resulting impurity scheme provides an excellent formalism to model and parametrize the LDOS at an arbitrary substitutional impurity site in the solid state [68].

One of the consequences of this approach is that the LDOS at a metalloid impurity site in a transition metal is, within the *single-band* formalism of the Clogston–Wolff model, very well understood in terms of a single parameter, namely an effective potential, which acts on the *metal* sp states. The hybridization gap in the metalloid LDOS follows therefore as a characteristic of the host material, and reflects the shape and position of the gap (already) present in the unperturbed transition metal sp states.

Acknowledgments

We gratefully acknowledge enlightening discussions with W Speier. This work was supported by the Stichting Scheikundig Onderzoek Nederland (SON) with financial aid from the Nederlandse Organisatie voor Wetenschappelijk Onderzoek (NWO).

References

[1] Terakura K, 1977 *J. Phys. F: Met. Phys.* **7** 1773
[2] Gelatt Jr C D, Williams A R and Moruzzi V L 1983 *Phys. Rev.* B **27** 2005
[3] Malozemoff A P, Williams A R and Moruzzi V L 1984 *Phys. Rev.* B **29** 1620
[4] Tanaka K, Matsumoto M, Oono S and Hiraki A 1975 *Appl. Phys. Lett.* **22** 529
[5] Fuggle J C, Källne E, Watson L M and Fabian D J 1977 *Phys. Rev.* B **16** 750
[6] Riley J D, Ley L, Azoulay J and Terakura K 1979 *Phys. Rev.* B **20** 776
[7] Fuggle J C, Hillebrecht F D, Zeller R, Zolnierek Z, Bennett P A and Freiburg Ch 1982 *Phys. Rev.* B **27** 2145
[8] Weaver J H, Franciosi A and Moruzzi V L *Phys. Rev.* B **29** 3293
[9] Sham T K 1985 *Phys. Rev.* B **31** 1903
[10] Sarma D D, Hillebrecht F U, Campagna M, Carbone C, Nogami J, Lindau I, Barbee T W, Braicovich L, Abbati I and De Michelis B 1985 *Z. Phys.* B **59** 159
[11] Tanaka K, Saito T, Suzuki K and Hasegawa R 1985 *Phys. Rev.* B **32** 6853
[12] Bisi O, Jepsen O and Andersen O K 1987 *Phys. Rev.* B **36** 9439
[13] Speier W, van Leuken E, Fuggle J C, Sarma D D, Kumar L, Dauth B and Buschow K H J 1989 *Phys. Rev.* B **39** 6008
Speier W, Kumar L, Sarma D D, de Groot R A and Fuggle J C 1989 *J. Phys.: Condens. Matter* **1** 9117
[14] Sarma D D, Speier W, Zeller R, van Leuken E, de Groot R A and Fuggle J C 1989 *J. Phys.: Condens. Matter* **1** 9131
[15] Weijs P J W, Czyżyk M T, Fuggle J C, Speier W, Sarma D D and Buschow K H J 1990 *Z. Phys.* B **78** 423
[16] Anderson P W 1961 *Phys. Rev.* **124** 41
[17] Moriya T 1965 *Prog. Theor. Phys.* **34** 329
[18] Heeger A J 1969 *Solid State Phys.* **23** 283
[19] Kondo F 1969 *Solid State Phys.* **23** 183
[20] Grüner G and Zawadowski A 1974 *Rep. Prog. Phys.* **37** 1497
[21] Terakura K and Kanamori J 1971 *Prog. Theor. Phys.* **46** 1007
Terakura K 1976 *J. Phys. Soc. Japan* **40** 450
[22] Fano U 1961 *Phys. Rev.* **124** 1866
[23] Friedel J 1958 *Nuovo Cimento Suppl.* **7** 287
[24] See e.g. Ziman J 1972 *Principles of the Theory of Solids* (Cambridge: Cambridge University Press) p 157
[25] Nieuwenhuys G J 1975 *Adv. Phys.* **24** 515, and references therein
[26] Kittel C 1968 *Solid State Phys.* **22** 1
[27] Moruzzi V L, Janak J F and Williams A R 1978 *Calculated Electronic Properties of Metals* (Oxford: Pergamon)
[28] Harrison W A 1980 *Electronic Structure and the Properties of Solids* (San Fransisco: Freeman)
[29] Borstel G 1985 *Appl. Phys.* A **38** 193
[30] Yeh J J and Lindau I 1985 *At. Data Nucl. Data Tables* **32** 2
[31] Cooper J W 1962 *Phys. Rev.* **128** 681
[32] Stöhr J, McFeely F R, Apai G, Wehner P S and Shirley D A 1976 *Phys. Rev.* B **14** 4431
[33] Shevchik N J 1977 *J. Phys. C: Solid State Phys.* **10** L555; 1977 *Phys. Rev.* B **16** 3428
[34] Winter H, Durham P J and Stocks G M 1984 *J. Phys. F: Met. Phys.* **14** 1047
[35] Speier W, Fuggle J C, Durham P J, Zeller R, Blake R J and Sterne P 1988 *J. Phys. C: Solid State Phys.* **21** 2621
[36] Rossi G, Lindau I, Braicovich L and Abbati I 1983 *Phys. Rev.* B **28** 3031
[37] Hedin L and Lundqvist S 1969 *Solid State Phys.* **23** 1
[38] Jackson W B and Allen J W 1980 *Phys. Rev.* B **37** 4618
[39] Liebsch A 1979 *Phys. Rev. Lett.* **43** 1431; 1981 *Phys. Rev.* B **23** 5203
[40] Hüfner S, Wertheim G K and Wernick J H 1975 *Solid State Commun.* **17** 1585
[41] Bosch A, Feil H, Sawatzky G A and Julianus J A 1984 *J. Phys. F: Met. Phys.* **14** 2225
[42] van der Marel D, Westra C, Sawatzky G A and Hillebrecht F U 1985 *Phys. Rev.* B **31** 1936
[43] van der Marel D, Julianus J A and Sawatzky G A 1985 *Phys. Rev.* B **32** 6331
[44] Folkerts W, van der Marel D, Haas C, Sawatzky G A, Norman D, Padmore H, Wright H and Weightman P 1987 *J. Phys. F: Met. Phys.* **17** 657
[45] van Acker J F, Weijs P W J, Fuggle J C, Horn K, Wilke W, Haak H, Saalfeld H, Kuhlenbeck

H, Braun W, Williams G P, Wesner D, Strongin M, Krummacher S and Buschow K H J 1988 *Phys. Rev.* B **38** 10463
[46] Fuggle J C and van Acker J P 1988 *J. Physique Coll.* **49** C8 25
[47] Watson L M, Kapoor Q S and Nemoshkalenko V V 1971 *J. Physique Coll.* **32** C4 325
[48] Oelhafen P 1983 *Glassy Metals vol II (Topics in Applied Physics 53)* ed H Beck and H-J Güntherodt (Berlin: Springer) p 283
[49] Smithells C J 1976 *Metals Reference Book* 5th edn (London: Butterworths)
[50] Amamou A, Aliaga-Guerra D, Panissod P, Krill G and Kuentzler R 1980 *J. Physique Coll.* **41** C8 396
[51] Mahan G D 1967 *Phys. Rev.* **163** 612
Nozières P and De Dominicis C T 1969 *Phys. Rev.* **178** 1097
[52] Müller J E, Jepsen O and Wilkins J W 1982 *Solid State Commun.* **42** 365
Müller J E and Williams J W 1984 *Phys. Rev.* B **29** 4331
[53] Fink J, Müller-Heinzerling Th, Scheerer B, Speier W, Hillebrecht F U, Fuggle J C, Zaanen J and Sawatzky G A 1985 *Phys. Rev.* B **32** 4899
[54] Zaanen J, Sawatzky G A, Fink J, Speier W and Fuggle J C 1985 *Phys. Rev.* B **32** 4905
[55] von Barth U and Grossmann G 1979 *Solid State Commun.* **32** 645
[56] Mahan G D 1980 *Phys. Rev.* B **21** 1421
[57] Ramaker D E, Hutson F L, Turner N H, Mei W N 1986 *Phys. Rev.* B **33** 2574
[58] Weijs P J W, Czyżyk M T, van Acker J F, Speier W, Goedkoop J B, van Leuken H, Hendrix H J M, de Groot R A, van der Laan G, Buschow K H J, Wiech G and Fuggle J C 1990 *Phys. Rev.* B **41** 11899
[59] Podloucky R, Zeller R and Dederichs P H 1980 *Phys. Rev.* B **22** 5777
[60] Shirley D A 1972 *Chem. Phys. Lett.* **16** 220
[61] Speier W, Fuggle J C, Zeller R, Ackermann B, Szot K, Hillebrecht F U and Campagna M 1984 *Phys. Rev.* B **30** 6921
[62] Grunes L A 1983 *Phys. Rev.* B **27** 2111
[63] Sham T K 1985 *Phys. Rev.* B **31** 1888
[64] Grebennikov V I, Babanov Yu A and Sokolov O B 1977 *Phys. Status Solidi* b **79** 423; 1977 *Phys. Status Solidi* b **80** 73
[65] Braspenning P J, Zeller R, Lodder A and Dederichs P H 1984 *Phys. Rev.* B **29** 703
[66] Clogston A M, Matthias B T, Peter M, Williams H J, Corenzwit E and Sherwood R J 1962 *Phys. Rev.* B **125** 541
[67] Drchal V and Kudrnovský J 1981 *Phys. Status Solidi* b **108** 683
[68] Speier W, van Acker J F and Zeller R 1990 *Phys. Rev.* **41** 2753